Water and ion diffusion in partially-water saturated compacted kaolinite: role played by vapor-phase diffusion in water mobility

Jingyi Wang, Sebastien Savoye, Eric Ferrage, Fabien Hubert, Serge Lefevre, Jean Radwan, Jean-Charles Robinet, Emmanuel Tertre, Philippe Gouze

Water and ion diffusion in partially-water saturated compacted kaolinite: role played by vapor-phase diffusion in water mobility

J. Wang[1],[2], S. Savoye[1], E. Ferrage[3], F. Hubert[3], S. Lefevre[1], J. Radwan[1], J.C. Robinet[4], E. Tertre[3], P. Gouze[2]

(1) Université Paris-Saclay, CEA, Service d'Etude du Comportement des Radionucléides, 91191 Gif-sur Yvette, France

(2) Géosciences Montpellier, CNRS-INSU - Montpellier University, 34095, Montpellier Cedex 5, France

(3) Université de Poitiers/CNRS, UMR 7285 IC2MP, Equipe HydrASA, 5 rue Albert Turpain, Bât. B8, TSA - 51106, 86073 Poitiers cedex 9, France

(4) R&D Division, Transfer Unit, Andra, 92298 Chatenay-Malabry, France

Abstract: Diffusion is the main transport process of water and solutes in clay-rich porous media owing to their very low permeability, so they are widely used as barriers against contaminant spreading. However, the prediction of contaminant mobility can be very complicated when these media are partially water-saturated. We conducted diffusion experiments for water (HTO and HDO) and ions ($^{22}Na^{+}$ and $^{125}I^{-}$) through partially water saturated compacted kaolinite, a weakly charged clay material, to quantify the distinct diffusive behavior of these species. The osmosis method was used to set kaolinite samples at 67, 86 and 100% saturation. The results showed that desaturation led to a sharp decrease in diffusive rates by factors of 6.5, 18 and 35 for HTO, $^{125}I^{-}$ and $^{22}Na^{+}$, respectively, from 100 to 67% of the degree of saturation. Thus, to interpret water diffusivities, we proposed a model taking into account the diffusion of water in both gas and liquid phases, using diffusion data obtained for ions, considered as inert species. This model was capable of properly predicting water diffusive flux, especially at a low degree of saturation (67% saturation), for which the assumption made for the occurrence of air phase continuity throughout the sample appears to be more relevant than at 86% saturation.

Key words: unsaturated water conditions; diffusion; kaolinite; osmotic method; water tracers; $^{125}I^{-}$; $^{22}Na^{+}$

Highlights:

- Decrease of water and ion diffusion in partially-water saturated kaolinite
- Significant discrepancy of water and ion diffusivity in unsaturated conditions
- No significant increase of surface diffusion when dehydrating
- A double diffusion model was developed for predicting water diffusion data

1. INTRODUCTION

Owing to their high retention capacity and their very low permeability, clay-rich media are widely used as barriers against contaminant spreading in many fields. Disposal facilities for high- and intermediate level long-lived radioactive waste, in many proposed designs, rely on swelling clay materials as engineered barriers (Bucher and Müller-Vonmoos, 1989; Landais, 2006) and some disposal facilities should also be directly sited in deep argillaceous formations (ANDRA, 2005; Hendry et al., 2015; Rao et al., 2021). Liners used in subsurface waste landfills are usually made of clay materials (Foose et al., 2002; Katsumi et al., 2001). In the geological storage of CO_2 in saline aquifers or depleted oil/gas reservoirs, clay layers serve as caprocks to prevent any CO_2 leakage (Berthe et al., 2011).

In all of these cases, diffusion is the main process responsible for the transport of water and solutes over geological timescales (Descostes et al., 2008; Motellier et al., 2007; Van Loon et al., 2004). In existing studies dealing with the determination of diffusive parameters within these clay-rich media, water tracers, especially tritiated water (HTO), are generally considered as reference tracer for diffusion (Melkior et al., 2009; Tertre et al., 2018). Once the effective diffusion coefficient (D_e) of HTO is acquired, the diffusion rate of anion and cation species can be inferred by taking into account the electrostatic effects induced by the presence of charges at the clay surface. Electrostatic effects are responsible for the phenomenon of surface diffusion for cation species (Lehikoinen et al., 1995; Savoye et al., 2015) and the phenomenon of anion exclusion for anion species (Gvirtzman and Gorelick, 1991; Tournassat and Steefel, 2019; Van Loon et al., 2007).

However, there are many situations wherein these clay-rich porous media can be partially water-saturated. The generation of hydrogen due to the corrosion of canisters may dehydrate host rocks and engineered barriers made of swelling clay materials for more than 100,000 years in deep geological waste disposal facilities (Marschall et al., 2005). Additionally, clay liners

placed above the groundwater table are generally unsaturated, especially for landfills located in arid environments (Katsumi et al., 2001). Due to the CO_2 intrusion into caprocks in carbon geosequestration, caprocks can also be partially saturated (Minardi et al., 2021; Xiao et al., 2020). In these cases, understanding and parameterizing the diffusion processes under partially saturated media is required to evaluate the performance of the clay system and support engineering purposes. This is a challenging task, as illustrated by the fact that only a few studies have been reported in the literature. For instance, Nunn et al. (2018) presented a new method using X-ray radiography and iodide tracers for quantifying the degree of partial saturation of shale samples and measuring D_e. They showed that the D_e value decreased by 22% when saturation decreased from 100% to 93.3%.

Savoye et al. developed an original approach to perform diffusion experiments under partially saturated conditions in illite-sand mixtures (Savoye et al., 2014) and in Callovo-Oxfordien claystones, envisaged to host a French disposal facility for high- and intermediate level long-lived radioactive waste (Savoye et al., 2017, 2012, 2010). The osmotic method was used to control the partial saturated conditions of the clayey samples over the duration of diffusion experiments. They observed in Callovo-Oxfordien claystones a sharp drop in the D_e values for HTO, $^{125}I^-$ and $^{22}Na^+$ by factors of 6, 50 and 17, respectively, under conditions of 81% water saturation compared to full saturation conditions. The strong decrease in D_e for iodide was explained by the anion exclusion phenomenon that restricted iodide to the largest pores where dehydration was more pronounced. Nevertheless, the distinct behavior of D_e evolution for HTO and sodium was still speculative. Two different processes for which their relative contribution requires further investigation were proposed. On the one hand, the extent of surface diffusion may be attenuated when dehydration occurs in claystones, reducing the enhanced diffusion phenomenon for cation species (Savoye et al., 2012). On the other hand, in addition to HTO diffusing in the liquid phase, HTO diffusing in vapor form may contribute to the relatively high

(compared to sodium) HTO diffusive rate, even at 81% water saturation (Savoye et al., 2017). This latter process was proposed by Smiles et al. (1995) and more recently by Maples et al. (2013) to explain the anomalously widespread distribution of HTO in layers adjacent to low-level radioactive waste burial facilities. Then, even though surface effect can be enhanced when saturation decreases (Churakov, 2013; Le Crom, 2020), the evolution of enhanced diffusion phenomenon for cation species when dehydrating is still an open question.

Therefore, the motivation of the current study is to acquire and discuss diffusion data (water and ionic tracers) under partially-saturated conditions with kaolinite, a weakly charged clay mineral compared to most of clay minerals present in Callovo-Oxfordian claystones (Claret et al., 2004). Three degrees of water saturation were achieved by means of the osmotic method. The results are discussed in light of previous studies performed in Callovo-Oxfordian claystones, and a model taking into account diffusion in both vapor and liquid phases was applied to interpret the results for water tracers.

2. MATERIALS AND METHODS

2.1. Materials and sample preparation

The kaolinite sample used in this study is the KGa-2 kaolinite, which was originally sourced by the University of Western Australia from the Source Clay Repository of the Clay Mineral Society. KGa-2 kaolinite has an average particle size of approximately 0.5 µm (Hassan et al., 2006), a specific area of 10.05 ± 0.02 m2/g (BET N2 method) and a corresponding CEC of 2.0 meq/100 g clay (Au et al., 2015). Its structural formula is $[(Al_{3.80}Ti_{0.13}Fe^{3+}_{0.07})(Si_{3.84}Al_{0.16})O_5(OH_4)]$ (Mermut, 2001). The mineralogy of KGa-2 consists of approximately 96 wt% kaolinite, 3 wt% anatase, and 1 wt% crandallite with trace amounts of mica and/or illite (Chipera, 2001). The KGa-2 used in our study is Na-saturated, and the preparation procedure is detailed in Dabat et al. (2020).

The diffusion tests under partially saturated conditions were performed with a through-diffusion set-up adapted from that used by Tertre et al. (2018). Three 10-mm-thick samples were directly prepared in the diffusion cells by compacting kaolinite powder in a body cell with a 9.49 mm inner diameter. The total porosity of the sample was evaluated according to the following equation:

$$\phi = 1 - \frac{\rho_d}{\rho_s} \quad (1.)$$

where ρ_s denotes the measured grain density of the sample: 2600 kg m^{-3} (Hassan et al., 2006; Tertre et al., 2018), and ρ_d is the dried bulk density. In our study, kaolinite samples compacted at a dried bulk density of 1950 kg m^{-3} displayed a total porosity ϕ of 25 (± 2) %.

Moreover, the volumetric moisture content, θ, was evaluated by using the following expression (Savoye et al., 2006) :

$$\theta = \frac{\omega \times \rho_s}{(1-\omega) \times \rho_w + \omega \times \rho_s} \quad (2.)$$

where ω is the water content of the sample, and ρ_w is the density of the pore water (assumed to be 1000 kg m^{-3}). The saturation degree (S_w) was further calculated as the ratio of volumetric water content to the total porosity:

$$S_w = \frac{\theta}{\phi} \quad (3.)$$

2.2. Procedure for setting saturation and petrophysical measurements

Different degrees of water saturation for kaolinite samples were achieved via the osmosis method. In this method, a solution concentrated in large-size molecules of polyethylene glycol (PEG) and a type of semipermeable membrane (Spectra por 3500 Da, Spectrum laboratories), which is permeable to all solutes except PEG, were applied. The membranes were installed on both sides of the kaolinite sample to separate the clay sample from the infiltrating solutions, some of which were PEG-rich. The semipermeable membranes prevent the PEG molecules

131 from entering the sample cell, thus inducing a controlled difference in PEG concentration
132 between the clay pore solution and that in the reservoir chambers. The difference in PEG
133 concentration triggers a suction process that prevents the solution from fully infiltrating the dry
134 kaolinite sample and hence, keeps it in a partially saturated state throughout the duration of the
135 diffusion experiments (more details of the method can be found in Savoye et al. (2010). Note
136 that the final value of the degree of saturation for samples depends on the PEG concentration
137 in the infiltrating solution, as shown by Delage and Cui (2008). In our study, suction values of
138 0 MPa, 1.9 MPa and 9 MPa were achieved by using solutions with PEG concentrations of 0,
139 0.42 and 0.95 g PEG/g water, respectively.
140 The hydric procedure lasted approximately 30 days, which is the same duration as that
141 mentioned by Savoye et al., (2014, 2010) for illite/sand and Callovo-Oxfordian claystone
142 samples. For the preparation of solutions, PEG 6000 (Merck, Germany) was added to NaCl
143 100 mM solutions beforehand, prepared with ultrapure deionized water (18 MΩ cm−1) and
144 commercial NaCl salts (American Chemical Society (ACS)) to obtain the targeted PEG
145 concentrations. A 24-hour stirring was necessary for the total dissolution of PEG pills and their
146 homogenization with NaCl solutions.
147 To determine the values of the degree of saturation for the samples as a function of imposed
148 suctions, samples were weighed before and after oven-heating at 105 °C. The mass loss during
149 this heating process over the total dry mass gives the water content of the sample. This weight
150 measurement work was performed after the completion of through-diffusion tests and
151 dismantlement of the diffusion cells.
152 In parallel, two kaolinite samples having the same size as those used for through-diffusion
153 experiments were prepared to be used for another saturation method: the saline solution method.
154 This method is applied as an assessment for the osmotic method. Degrees of water saturation
155 of these two samples were set by controlling the environmental relative humidity of the cells

156 with a saturated saline solution. For that purpose, kaolinite powder was compacted within a cell
157 made of polypropylene, and the sample was sandwiched between two stainless steel filter
158 plates. The cell was first placed in a desiccator in which relative humidity was imposed by a
159 saturated saline solution of $BaCl_2$ (i.e., it fixed a humidity of approximately 90%). The mass of
160 the cell was monitored over time to determine the duration required to reach stabilization.
161 Afterward, the cell was moved into another desiccator with a saturated saline solution of
162 KH_2PO_4 (i.e., it fixed a humidity of approximately 96.5%). These two saline solutions provide
163 suction values equal to 15.1 and 7.3 MPa, according to Delage et al. (1998) and Lahsasni et al.
164 (2002).

165 **2.3. Through-diffusion experiment**

166 After the one-month hydric procedure, diffusion cells were connected to upstream and
167 downstream reservoirs. The upstream reservoir was filled with 25 g of 100 mM NaCl (without
168 considering PEG mass) solution spiked with specific tracers, i.e., HDO, HTO (labeled CERCA
169 ELSB45 n◦760,112/4), $^{22}Na^+$ (labeled ELSB45 80693/1), $^{125}I^-$ (labeled ELSB50 82731/1) or
170 $^{36}Cl^-$ (labeled E&Z 1760–100-1) were used to determine diffusion parameters for water, cation
171 and anion tracers. The initial activities injected in upstream solution for HTO, $^{36}Cl^-$, $^{125}I^-$ and
172 $^{22}Na^+$ were resp. 0.7 kBq/g, 0.5 kBq/g, 0.8 kBq/g and 0.2 kBq/g (without considering PEG
173 mass). In the case of $^{125}I^-$, stable iodide was added to reach a concentration of 10^{-3} M in the
174 upstream reservoir to avoid any strong uptake of iodine, as previously observed by Bazer-Bachi
175 et al. (2006) for lower concentrations ($< 10^{-4}$ M). Moreover, thiosulfate at a concentration of
176 5×10^{-4} M was also added to both reservoirs to ensure that iodide remained in the same redox
177 state (Descostes et al., 2008).

178 The solution in the downstream reservoir was systematically replaced to maintain the tracer
179 concentration as low as reasonably possible, i.e., less than 3% of the value measured in the
180 upstream reservoir. The activity or concentration of tracers in downstream samples was

181 measured via different techniques depending on the type of tracer. The concentration of HDO
182 in solution was measured by a liquid water isotope analyzer (LWIA DLT-100 from Los Gatos
183 Research) based on infrared spectroscopy. Activity for HTO and $^{36}Cl^-$ was measured by a
184 Packard Tri-Carb 2500 liquid scintillation recorder, while activity for $^{125}I^-$ and $^{22}Na^+$ was
185 measured using a gamma counter (Packard 1480 WIZARD).

186 For the diffusion cell at full saturation, HTO and $^{36}Cl^-$ were first injected at the same time.
187 Afterward, solutions in both reservoirs were replaced with fresh synthetic water without tracer
188 for the starting out-diffusion stage lasting up to 3 weeks. A through-diffusion test with $^{125}I^-$ was
189 launched as soon as the HTO out-diffusion flux was negligible, i.e., for a residual HTO activity
190 close to the detection limit (0.5 Bq). Then, $^{22}Na^+$ was immediately injected after the end of $^{125}I^-$
191 through-diffusion since their spectral peaks do not overlap in the measurement of the gamma
192 counter. Note that for the two anion tracers, $^{125}I^-$ was preferred to $^{36}Cl^-$ because of the lack of
193 waste management channels for organic solutions containing long-lived radionuclides, such as
194 $^{36}Cl^-$. For the two cells under partial-saturation conditions, HDO was first injected, followed
195 by $^{125}I^-$. Then, a $^{125}I^-$ out-diffusion step was carried out to allow the injection of HTO and $^{22}Na^+$
196 for the last stage, and the HTO measurement was sensitive to the presence of $^{125}I^-$.

197 **2.4. Treatment of experimental results**

198 The analysis of through-diffusion experiments is based on Fick's second law for one-
199 dimensional transport. Planar through-diffusion was assumed for all tracers, and their diffusion
200 was considered independent; that is, no chemical interactions existed between them. The
201 following form is hence applicable:

202 $$\frac{\partial C}{\partial t} = \frac{D_e}{\alpha}\frac{\partial^2 C}{\partial x^2} = \frac{D_e}{\theta_{diff}^t + \rho_d R_d}\frac{\partial^2 C}{\partial x^2} = \frac{D_e}{R\theta_{diff}^t}\frac{\partial^2 C}{\partial x^2} \quad (4.)$$

where C is given as the molar or activity concentration (mol m^{-3} of synthetic pore water without PEG or Bq m^{-3}); t is the time (s); D_e denotes the effective diffusion coefficient (m^2 s^{-1}), and α is the rock capacity factor:

$$\alpha = \theta_{diff}^{t} + \rho_d R_d \quad (5.)$$

where θ_{diff}^{t} is the volumetric water content accessible to the diffusing tracer (-); ρ_d is the dry bulk density (kg m^{-3}), and R_d is the distribution ratio (m^3 kg^{-3}). The capacity factor can be written as $R\theta_{diff}^{t}$ with R being the retardation factor:

$$R = 1 + \frac{\rho_d R_d}{\theta_{diff}^{t}} \quad (6.)$$

According to van Brakel and Heertjes (1974) and Grathwohl (1998), De can be expressed as a function of θ_{diff}^{t} as follows:

$$D_e = D_p \theta_{diff}^{t} = \frac{\delta}{\tau^2} D_0 \theta_{diff}^{t} = \frac{1}{G} D_0 \theta_{diff}^{t} \quad (7.)$$

where D_p denotes the pore diffusion coefficient (m^2 s^{-1}); D_0 denotes the self-diffusion coefficient in water (m^2 s^{-1}); δ represents the constrictivity factor (-), and τ is the tortuosity factor (-). Tortuosity and constrictivity are purely geometric factors that, compared with a specific cross-section in free water, lengthen the effective diffusion pathway and reduce the overall diffusion cross-section, respectively (van Brakel and Heertjes, 1974). G denotes the geometric factor (-).

The initial and boundary conditions are:

$C(x,t) = 0, \qquad t = 0$

$C(x,t) = C_0, \qquad x = 0, t > 0$

$C(x,t) = 0, \qquad x = L, t > 0$

where L is the sample thickness (m).

Fully analytical solutions of Equation 4 are given by Cranck (1975). The cumulative activity A_{diff}^{t} can be written as:

$$A_{diff}^{t} = S \cdot L \cdot A_0 \cdot \left[\frac{D_e t}{L^2} - \frac{\theta_{diff}^{t}}{6} - \frac{2\theta_{diff}^{t}}{\pi^2}\sum_{n=1}^{\infty}\frac{(-1)^2}{n^2} exp\left\{-\frac{D_e n^2 \pi^2 t}{L^2 \theta_{diff}^{t}}\right\}\right] \quad (8.)$$

and the incoming instantaneous flux of tracer F_i in the downstream reservoir is:

$$F_i = \frac{D_e A_0}{L}\left[1 + 2\sum_{n=1}^{\infty}(-1)^2 exp\left\{-\frac{D_e n^2 \pi^2 t}{L^2 \theta_{diff}^{t}}\right\}\right] \quad (9.)$$

where S is the surface of the sample perpendicular to the diffusion flux (m^2).

The analysis of the results was performed by least squares fitting of the model to the results of the incoming instantaneous flux in the downstream reservoir using Equation 9.(Savoye et al., 2015)

3. Results and discussion

3.1. Comparison of the values of saturation degree obtained *via* osmotic and saline solution methods

Figure 1 shows the values of water saturation degree of compacted kaolinite samples as a function of the values of imposed suction. The data points obtained by both methods are in rather good agreement: a gradual decrease in saturation degree can be observed when the imposed suction decreases. For the kaolinite samples dehydrated by the osmosis technique, the saturation degree values at suction levels of 1.9 and 9 MPa are 67 ($\pm$3) % and 86 ($\pm$5) %, corresponding to volumetric water content values of 0.17 ($\pm$0.01) and 0.215 ($\pm$0.0125), respectively.

3.2. Diffusion under fully saturated conditions

The normalized diffusive flux (in m s^{-1}) for water tracers (a, for HTO; b, for HDO), anion tracers (c, for $^{125}I^-$ and $^{36}Cl^-$) and cation tracers (d, for $^{22}Na^+$) under fully saturated conditions

247 are reported in Figure 2. Normalized flux was calculated for each tracer using the ratio of
248 instantaneous flux in Bq $m^{-2}s^{-1}$ (or mol $m^{-2}s^{-1}$ for HDO) over the concentration in the upstream
249 reservoir in Bq m^{-3} or mol m^{-3}. The corresponding values of effective diffusion coefficient, D_e,
250 estimated from Fick's law are reported in Table 1, as well as values of the rock capacity factor,
251 α and those of the distribution ratio, R_d. The D_e value for HTO is close to the values found by
252 Asaad et al. (2021) for the same porous medium compacted at the same dry bulk density, using
253 both through-diffusion and ^{1}H NMR pulsed gradient spin echo experiments, validating that our
254 through-diffusion setup was not influenced by using semipermeable membranes. As far as ions
255 are concerned, D_e values are similar to those reported by Glaus et al. (2010) for the same clay
256 porous material. Moreover, a low but significant retardation was observed for $^{36}Cl^{-}$, $^{125}I^{-}$ and
257 $^{22}Na^{+}$ (Table 1). This behavior was also reported by Glaus et al. (2010) for the same porous
258 medium and sodium aqueous concentration in porewater. Note that for anion species, positively
259 charged edge sites of kaolinite would be responsible for the adsorption of both anion species to
260 a similar extent, given that the pH of porewater used at approximately 5 is slightly lower that
261 the zero proton charge of KGa-2 (i.e., 5.5 according to Huertas et al., 1998).

262 For this full water saturation condition, effective diffusion coefficients obtained for water and
263 ions were normalized to their self-diffusion coefficients in bulk water, D_0, with
264 $D_{0,HTO} = 2.00 \times 10^{-9}$ m² s^{-1}, $D_{0,Cl-} = 1.77 \times 10^{-9}$ m² s^{-1}, $D_{0,I-} = 1.79 \times 10^{-9}$ m² s^{-1} and
265 $D_{0,Na+} = 1.17 \times 10^{-9}$ m² s^{-}1 (Li and Gregory, 1974; Savoye et al., 2011). These data, i.e.
266 diffusivities, are reported in Figure 3A. For the three tracers used, data are very similar,
267 indicating that the electrostatic effects would be too low to significantly impact the diffusive
268 rate of cation species *via* surface diffusion and anion species *via* anion exclusion, as already
269 shown by Glaus et al. (2010) and Rajyaguru et al. (2021). Conversely, in other clay media
270 dominated by illite layers (i.e., high charge layers), electrostatic effects become more
271 pronounced, leading to significant differences for the diffusivities between anions, cations and

neutral species. For example, as shown in Figure 3B, data reported for Callovo-Oxfordian claystones showed an enhanced diffusion for $^{22}Na^{+}$ and the mobility of $^{125}I^{-}$ is strongly slowed down compared to HTO. Then, by comparing data obtained in this study for kaolinite and for claystones rich in illite layers reported from literature, we can reasonably assume to neglect electrostatic effect of kaolinite in the interpretation of the diffusivities of different charged probes at full water saturation condition. However, question remaining opens for unsaturated conditions.

3.3. Effect of water saturation on tracer diffusive rate

For water and ions, Figure 2 (a-d) compares the normalized diffusive flux in m s^{-1} obtained at full saturation with those obtained at suction levels equal to 1.9 MPa and 9 MPa. As expected, a clear decrease of the diffusive rates was observed for all the tracers when suction increases. For example, diffusive flux rates decrease for suction values from 0 to 9 MPa by factors of 6.5, 18 and 35 for HTO, $^{125}I^{-}$ and $^{22}Na^{+}$, respectively. Corresponding values for D_e, α and R_d are reported in Table 1. R_d values obtained for unsaturated conditions are lower than those obtained at full saturation for both anion and cation, indicating that adsorption extent is reduced at lower water content.

Diffusivity data reported in Figure 3 show that HTO/HDO diffusion deviated from ions diffusivity when suction increases, contrary to data obtained at a full water saturation. At a suction of 9 MPa, the values of the ratio between water (HTO or HDO) and solute (iodide or sodium) diffusivity increase up to a range lying between 3 and 4 (see Table 2). This discrepancy between water and ions can originate from mobility either i) slowed down for ions or ii) enhanced for water tracers. Regarding the first assumption, some authors demonstrated by molecular dynamic simulations that self-diffusion coefficient of ions near the clay water interfaces under partially saturated conditions decreased compared to full saturated conditions

(Churakov 2013; Le Crom, 2019). Note that Churakov (2013) reports also significant increase of self-diffusion coefficient of water for similar conditions. This behavior combined with data obtained from other clayey materials (Savoye et al., 2017) allow us to explore the water-enhanced mobility assumption. This can be also justified due to the very low R_d values measured for ions under unsaturated conditions compared to full saturated one.

3.4. Application of a double-diffusion model in both vapor and liquid phases for water tracers

In this section, we present a model for water tracers enabling their diffusion to be taken into account in both liquid and gas phases. The total flux F is the sum of F_{liq}, the diffusive flux of the water tracer in liquid water, and F_{gas}, that in the gas phase, namely,

$$F = F_{liq} + F_{gas} \quad (10.)$$

According to Fick's law for porous media, the diffusive flux can be written as:

$$F = -D_{e,liq}\frac{\partial C_{liq}}{\partial x} + -D_{e,gas}\frac{\partial C_{gas}}{\partial x} \quad (11.)$$

On the one hand, the effective diffusion coefficient of water in the liquid phase, $D_{e,\,liq}$, was described by that of an inert tracer diffusing only in the liquid phase. Owing to R_d values close to zero under water unsaturated conditions for ions (Table 1), we used $D_{e,\,I-}$ or $D_{e,\,Na+}$, values measured experimentally at the corresponding levels of suction and corrected by considering their difference in the self-diffusion coefficient, D_0:

$$D_{e,liq} = D_{e,I-/Na+} \cdot \frac{D_{0,water\ tracer}}{D_{0,I-/Na+}} \quad (12.)$$

Such an approach assumes that the effect of medium organization (e.g., tortuosity/constrictivity) would be the same for liquid water and ions at a given degree of saturation.

On the other hand, for water diffusion in the gas phase, Equation 7 was modified to Equation 13 to estimate the effective diffusion coefficient in the gas phase, $D_{e,\,gas}$:

$$D_{e,gas} = \frac{1}{G} D_{0,gas}(\phi - \theta) \quad (13.)$$

$D_{0,\,gas}$ corresponds to the free vapor diffusion coefficient, equal to 2.6×10^{-5} m² s^{-1} (Maples et al., 2013; Smiles et al., 1995), and the porosity is equal to the air porosity, i.e., $\phi - \theta$, and the geometric factor value was determined at full saturation for water tracers. This last point means that a continuity of the gas phase in the whole pore network from the upstream to the downstream sides for the unsaturated samples was assumed.

In addition, exchange between liquid and gas phases is considered using Henry's law (Equation 14), yielding an equilibrium constant H (-) of 1.66×10^{-5} (at 22 °C and 100% relative humidity).

$$C_{gas} = HC_{liq} \quad (14.)$$

This exchange is assumed to be instantaneous, reversible and without significant fractionation between the different isotopes of the water molecules, as demonstrated by Savoye et al. (2018) for HTO.

The total flux F can thus be rewritten as:

$$F = F_{liq} + F_{gas} = -D_e^* \frac{\partial C_{liq}}{\partial x} \quad (15.)$$

where D_e^* is the effective diffusion coefficient (see Table 3 for the calculations of D_e^*):

$$D_e^* = D_{e,liq} + HD_{e,gas} \quad (16.)$$

In fact, mass exchange would occur at all liquid-gas interfaces, i.e., (i) at the upstream and downstream sides, between liquid water and the gas in contact with, and (ii) in the sample porosity. In pores, this liquid/gas exchange will induce a noticeable retardation for water tracers when water vapor diffuses in the air. This retardation can be estimated in the form of a retardation factor (see SI for its demonstration):

$$R_{gas/sol\_eq} = 1 + \frac{\theta}{H(1-\phi+\theta)(\phi-\theta)} \quad (17.)$$

HDO fluxes calculated by this model are plotted in Figure 4 and compared with experimental data obtained at 1.9 MPa and 9 MPa (see Table 3 for values of parameters applied in the model). At the lower saturation, i.e., 9 MPa of suction, the model allows the experimental flux to be well reproduced (both transient and steady states), independently of using either $D_{e,\,125I^-}$ or $D_{e,\,22Na^+}$ for $D_{e,\,liq}$ (Eq. 12). At this degree of saturation, the model suggests that the contribution of diffusion in the gas phase is predominant (see Figure 4). For higher water content (i.e., 1.9 MPa), the agreement between the model and experiment is still satisfying, especially when using $D_{e,\,125I^-}$ for $D_{e,\,liq}$. In this case, the contribution of diffusion in the gas phase would be minor.

The application of Jurin-Laplace's law for a suction of 1.9 MPa shows that pores with diameters less than 150 nm should be totally filled with liquid water, while the results of mercury intrusion porosimetry (MIP) indicated a mean pore throat value of approximately 35 nm for a sample of kaolinite compacted at a dried bulk density slightly lower than ours (1690 kg m^{-3}) (Rajyaguru et al., 2021). This means that most of the pores would be filled with liquid water, thus excluding a possible continuity of the gas phase through the whole pore network at 1.9 MPa. In this case, other processes, such as evapo-condensation, could also facilitate water

359 tracer diffusion. Conversely, at a suction of 9 MPa, since few pores would be totally water-
360 saturated (i.e., the pores with a diameter < 30 nm according to Jurin-Laplace's law), our
361 hypothesis assuming a gas phase continuity would therefore be more relevant.

362 ## 4. CONCLUSIONS

363 At full water saturation, we confirmed that the diffusivity values of water and ion tracers were
364 similar in compacted kaolinite. This justified the use of this clay mineral as a model system to
365 assess the evolution of surface diffusion phenomenon of ions with the decrease of water content.
366 As expected, effective diffusion coefficient values for water and ions decreased when suction
367 increased. However, contrary to the full water condition, diffusivity values for anion and cation
368 are significantly lower than those of water tracers. This demonstrates that the enhanced
369 diffusion phenomenon for cations did not occur in kaolinite at the water content values used in
370 this study. To account for the distinct diffusive behavior of water and ions based on diffusivity,
371 a model taking into account water diffusion in both the gas and liquid phases was proposed.
372 The assumption for the occurrence of air phase continuity throughout the sample appears to be
373 relevant for low saturation values, while it starts to fail to reproduce the data for saturation
374 higher than approximately 86%, for which direct 3D simulations are required.

375 Modeling diffusion in partially saturated clayey material remains highly challenging. The
376 experimental dataset provided in this study could be used for testing different simulation
377 approaches such as brownian dynamics (Dabat, 2019) or random walk methods (Russian et al.,
378 2017). These simulation approaches could also benefit from generated binary structures
379 mimicking the porosity of the clay porous materials used in this study (see Ferrage et al., 2015
380 with their disk-stacking pattern model) or kinetic Monte Carlo grain growth algorithm (Tyagi
381 et al., 2013). Alternative methods such as the augmented Young-Laplace approach (Philip,
382 1977), tested for clayey material by Gimmi and Churakov (2019) could also be considered.

Acknowledgement

The results presented are part of the Ph.D. thesis of J.W. granted by Andra and CEA. The authors are grateful to the CNRS interdisciplinary “défi Needs” through its “MiPor” program (Project DARIUS), and the European Union’s Horizon 2020 research and innovation program under Grant Agreement No. 847593. We also thank the two anonymous reviewers for their comments.

Reference

ANDRA, D., 2005. Argile: Évolution phénoménologique du stockage géologique, 2005.

Asaad, A., Hubert, F., Ferrage, E., Dabat, T., Paineau, E., Porion, P., Savoye, S., Gregoire, B., Dazas, B., Delville, A., Tertre, E., 2021. Role of interlayer porosity and particle organization in the diffusion of water in swelling clays. Appl. Clay Sci. 207, 106089. https://doi.org/10.1016/j.clay.2021.106089

Au, P.-I., Clode, P., Smart, R.St.C., Leong, Y.-K., 2015. Surface chemistry–microstructure–rheology of high and low crystallinity KGa-1b and KGa-2 kaolinite suspensions. Colloids Surf. Physicochem. Eng. Asp. 484, 354–364. https://doi.org/10.1016/j.colsurfa.2015.08.013

Bazer-Bachi, F., Tevissen, E., Descostes, M., Grenut, B., Meier, P., Simonnot, M.-O., Sardin, M., 2006. Characterization of iodide retention on Callovo-Oxfordian argillites and its influence on iodide migration. Phys. Chem. Earth Parts ABC 31, 517–522. https://doi.org/10.1016/j.pce.2006.04.015

405 Berthe, G., Savoye, S., Wittebroodt, C., Michelot, J.-L., 2011. Changes in containment
406 properties of claystone caprocks induced by dissolved CO_2 seepage. Energy Procedia
407 4, 5314–5319. https://doi.org/10.1016/j.egypro.2011.02.512
408 Bucher, F., Müller-Vonmoos, M., 1989. Bentonite as a containment barrier for the disposal of
409 highly radioactive wastes. Appl. Clay Sci. 4, 157–177. https://doi.org/10.1016/0169-
410 1317(89)90006-9
411 Chipera, S.J., 2001. Baseline Studies of the Clay Minerals Society Source Clays: Powder X-
412 ray Diffraction Analyses. Clays Clay Miner. 49, 398–409.
413 https://doi.org/10.1346/CCMN.2001.0490507
414 Churakov, S.V., 2013. Mobility of Na and Cs on Montmorillonite Surface under Partially
415 Saturated Conditions. Environ. Sci. Technol. 47, 9816–9823.
416 https://doi.org/10.1021/es401530n
417 Claret, F., Sakharov, B.A., Drits, V.A., Velde, B., Meunier, A., Griffault, L., Lanson, B.,
418 2004. Clay minerals in the Meuse-Haute Marne underground laboratory (France):
419 possible influence of organic matter on clay mineral evolution Clays Clay Miner. 52,
420 515-532. https://doi.org/10.1346/CCMN.2004.0520501
421 Crank, J., 1975. The mathematics of diffusion, 2nd ed. Clarendon Press, Oxford Science
422 Publication : New York.
423 Dabat, T., 2019. Anisotropie des milieux poreux argileux et implication sur la diffusion de
424 l'eau (PhD). Université de Poitiers, France.
425 Dabat, T., Porion, P., Hubert, F., Paineau, E., Dazas, B., Grégoire, B., Tertre, E., Delville, A.,
426 Ferrage, E., 2020. Influence of preferred orientation of clay particles on the diffusion
427 of water in kaolinite porous media at constant porosity. Appl. Clay Sci. 184, 105354.
428 https://doi.org/10.1016/j.clay.2019.105354

Delage, P., Cui, Y.J., 2008. An evaluation of the osmotic method of controlling suction∗. Geomech. Geoengin. 3, 1–11. https://doi.org/10.1080/17486020701868379

Delage, P., Howat, M.D., Cui, Y.J., 1998. The relationship between suction and swelling properties in a heavily compacted unsaturated clay. Eng. Geol. 50, 31–48. https://doi.org/10.1016/S0013-7952(97)00083-5

Descostes, M., Blin, V., Bazer-Bachi, F., Meier, P., Grenut, B., Radwan, J., Schlegel, M.L., Buschaert, S., Coelho, D., Tevissen, E., 2008. Diffusion of anionic species in Callovo-Oxfordian argillites and Oxfordian limestones (Meuse/Haute–Marne, France). Appl. Geochem. 23, 655–677. https://doi.org/10.1016/j.apgeochem.2007.11.003

Ferrage, E., Hubert, F., Tertre, E., Delville, A., Michot, L.J., Levitz, P., 2015. Modeling the arrangement of particles in natural swelling-clay porous media using three-dimensional packing of elliptic disks. Phys. Rev. E 18.

Foose, G.J., Benson, C.H., Edil, T.B., 2002. Comparison of Solute Transport in Three Composite Liners. J. Geotech. Geoenvironmental Eng. 128, 391–403. https://doi.org/10.1061/(ASCE)1090-0241(2002)128:5(391)

Gimmi, T., Churakov, S.V., 2019. Water retention and diffusion in unsaturated clays: Connecting atomistic and pore scale simulations. Appl. Clay Sci. 175, 169–183. https://doi.org/10.1016/j.clay.2019.03.035

Glaus, M.A., Frick, S., Rossé, R., Loon, L.R.V., 2010. Comparative study of tracer diffusion of HTO, $^{22}Na^{+}$ and $^{36}Cl^{-}$ in compacted kaolinite, illite and montmorillonite. Geochim. Cosmochim. Acta 74, 1999–2010. https://doi.org/10.1016/j.gca.2010.01.010

Grathwohl, P., 1998. Modelling of Diffusion Processes, in: Diffusion in Natural Porous Media. Springer, pp. 43–81.

Gvirtzman, H., Gorelick, S.M., 1991. Dispersion and advection in unsaturated porous media enhanced by anion exclusion. Nature 352, 793–795. https://doi.org/10.1038/352793a0

Hassan, M.S., Villieras, F., Gaboriaud, F., Razafitianamaharavo, A., 2006. AFM and low-pressure argon adsorption analysis of geometrical properties of phyllosilicates. J. Colloid Interface Sci. 296, 614–623. https://doi.org/10.1016/j.jcis.2005.09.028

Hendry, M.J., Solomon, D.K., Person, M., Wassenaar, L.I., Gardner, W.P., Clark, I.D., Mayer, K.U., Kunimaru, T., Nakata, K., Hasegawa, T., 2015. Can argillaceous formations isolate nuclear waste? Insights from isotopic, noble gas, and geochemical profiles. Geofluids 15, 381–386. https://doi.org/10.1111/gfl.12132

Huertas, F.J., Chou, L., Wollast, R., 1998. Mechanism of Kaolinite Dissolution at Room Temperature and Pressure: Part 1. Surface Speciation. Geochim. Cosmochim. Acta 62, 417–431. https://doi.org/10.1016/S0016-7037(97)00366-9

Katsumi, T., Benson, C.H., Foose, G.J., Kamon, M., 2001. Performance-based design of landfill liners. Eng. Geol., Geoenvironmental Engineering 60, 139–148. https://doi.org/10.1016/S0013-7952(00)00096-X

Lahsasni, S., Kouhila, M., Mahrouz, M., Kechaou, N., 2002. Experimental study and modelling of adsorption and desorption isotherms of prickly pear peel (Opuntia ficus indica). J. Food Eng. 55, 201–207. https://doi.org/10.1016/S0260-8774(02)00064-X

Landais, P., 2006. Advances in geochemical research for the underground disposal of high-level, long-lived radioactive waste in a clay formation. J. Geochem. Explor. 88, 32–36. https://doi.org/10.1016/j.gexplo.2005.08.011

Le Crom, S., 2019. Modélisation à l'échelle microscopique des fluides et des solutés dans des argiles saturées et insaturées. Ph D dissertation of Paris Sorbonne University, France.

Lehikoinen, J., Carlsson, T., Muurinen, A., Olin, M., Salonen, P., 1995. Evaluation of Factors Affecting Diffusion in Compacted Bentonite. MRS Proc. 412, 675. https://doi.org/10.1557/PROC-412-675

Li, Y.-H., Gregory, S., 1974. Diffusion of ions in sea water and in deep-sea sediments. Geochim. Cosmochim. Acta 38, 703–714.

Maples, S.R., Andraski, B.J., Stonestrom, D.A., Cooper, C.A., Pohll, G., Michel, R.L., 2013. Tritium Plume Dynamics in the Shallow Unsaturated Zone in an Arid Environment. Vadose Zone J. 12, vzj2013.05.0080. https://doi.org/10.2136/vzj2013.05.0080

Marschall, P., Horseman, S., Gimmi, T., 2005. Characterisation of Gas Transport Properties of the Opalinus Clay, a Potential Host Rock Formation for Radioactive Waste Disposal. Oil Gas Sci. Technol. 60, 121–139. https://doi.org/10.2516/ogst:2005008

Melkior, T., Gaucher, E.C., Brouard, C., Yahiaoui, S., Thoby, D., Clinard, Ch., Ferrage, E., Guyonnet, D., Tournassat, C., Coelho, D., 2009. Na^+ and HTO diffusion in compacted bentonite: Effect of surface chemistry and related texture. J. Hydrol. 370, 9–20. https://doi.org/10.1016/j.jhydrol.2009.02.035

Mermut, A.R., 2001. Baseline Studies of the Clay Minerals Society Source Clays: Chemical Analyses of Major Elements. Clays Clay Miner. 49, 381–386. https://doi.org/10.1346/CCMN.2001.0490504

Minardi, A., Giger, S.B., Ewy, R.T., Stankovic, R., Stenebråten, J., Soldal, M., Rosone, M., Ferrari, A., Laloui, L., 2021. Benchmark study of undrained triaxial testing of Opalinus Clay shale: Results and implications for robust testing. Geomech. Energy Environ. 25, 100210. https://doi.org/10.1016/j.gete.2020.100210

Motellier, S., Devol-Brown, I., Savoye, S., Thoby, D., Alberto, J.-C., 2007. Evaluation of tritiated water diffusion through the Toarcian clayey formation of the Tournemire experimental site (France). J. Contam. Hydrol. 94, 99–108. https://doi.org/10.1016/j.jconhyd.2007.05.012

Nunn, J.A., Xiang, Y., Al, T.A., 2018. Investigation of partial water saturation effects on diffusion in shale. Appl. Geochem. 97, 93–101. https://doi.org/10.1016/j.apgeochem.2018.08.004

Philip, J.R., 1977. Unitary approach to capillary condensation and adsorption. J. Chem. Phys. 66, 5069–5075. https://doi.org/10.1063/1.433814

Rajyaguru, A., 2018. Impact of saline plume on containment properties of natural porous materials in geological disposal context: An experimental and REV simulation approach to go beyond Archie's law 319. Ph D dissertation of Mines Paris Tech, France.

Rajyaguru, A., Wang, J., Wittebroodt, C., Bildstein, O., Detilleux, V., Lagneau, V., Savoye, S., 2021. Barite precipitation in porous media: Impact of pore structure and surface charge on ionic diffusion. J. Contam. Hydrol. 242, 103851. https://doi.org/10.1016/j.jconhyd.2021.103851

Rao, Z., Li, G., Liu, X., Liu, P., Li, H., Liu, S., Zhu, M., Guo, C., Ni, F., Gong, Z., Asghar, F., 2021. Fault Activity in Clay Rock Site Candidate of High Level Radioactive Waste Repository, Tamusu, Inner Mongolia. Minerals 11, 941. https://doi.org/10.3390/min11090941

Russian, A., Dentz, M., Gouze, P., 2017. Self-averaging and weak ergodicity breaking of diffusion in heterogeneous media. Phys. Rev. E 96, 022156. https://doi.org/10.1103/PhysRevE.96.022156

Savoye, S., Michelot, J., Wittebroodt, C., Altinier, M.V., 2006. Contribution of the diffusive exchange method to the characterization of pore-water in consolidated argillaceous rocks. J. Contam. Hydrol. 86, 87–104. https://doi.org/10.1016/j.jconhyd.2006.02.010

Savoye, S., Page, J., Puente, C., Imbert, C., Coelho, D., 2010. New Experimental Approach for Studying Diffusion through an Intact and Unsaturated Medium: A Case Study with

526 Callovo-Oxfordian Argillite. Environ. Sci. Technol. 44, 3698–3704.
527 https://doi.org/10.1021/es903738t
528 Savoye, S., Goutelard, F., Beaucaire, C., Charles, Y., Fayette, A., Herbette, M., Larabi, Y.,
529 Coelho, D., 2011. Effect of temperature on the containment properties of argillaceous
530 rocks: The case study of Callovo–Oxfordian claystones. J. Contam. Hydrol. 125, 102–
531 112. https://doi.org/10.1016/j.jconhyd.2011.05.004
532 Savoye, S., Frasca, B., Grenut, B., Fayette, A., 2012. Mobility of cesium through the Callovo-
533 Oxfordian claystones under partially saturated conditions. Environ. Sci. Technol. 46,
534 2633–2641.
535 Savoye, S., Imbert, C., Fayette, A., Coelho, D., 2014. Experimental study on diffusion of
536 tritiated water and anions under variable water-saturation and clay mineral content:
537 comparison with the Callovo-Oxfordian claystones. Geol. Soc. Lond. Spec. Publ. 400,
538 579–588. https://doi.org/10.1144/SP400.9
539 Savoye, S., Beaucaire, C., Grenut, B., Fayette, A., 2015. Impact of the solution ionic strength
540 on strontium diffusion through the Callovo-Oxfordian clayrocks: An experimental and
541 modeling study. Appl. Geochem. 61, 41–52.
542 https://doi.org/10.1016/j.apgeochem.2015.05.011
543 Savoye, S., Lefevre, S., Fayette, A., Robinet, J.-C., 2017. Effect of Water Saturation on the
544 Diffusion/Adsorption of ^{22}Na and Cesium onto the Callovo-Oxfordian Claystones.
545 Geofluids 2017, 1–17. https://doi.org/10.1155/2017/1683979
546 Savoye, S., Rajyaguru, A., Mace, N., Lefevre, S., Spir, G., Robinet, J.-C., 2018. How mobile
547 is tritiated water through unsaturated cement-based materials? New insights from two
548 complementary approaches. Appl. Radiat. Isot. 139, 98–106.
549 Smiles, D.E., Gardner, W.R., Schulz, R.K., 1995. Diffusion of tritium in arid disposal sites.
550 Water Resour. Res. 31, 1483–1488. https://doi.org/10.1029/94WR02013

551 Tertre, E., Savoye, S., Hubert, F., Prêt, D., Dabat, T., Ferrage, E., 2018. Diffusion of Water
552 through the Dual-Porosity Swelling Clay Mineral Vermiculite. Environ. Sci. Technol.
553 52, 1899–1907. https://doi.org/10.1021/acs.est.7b05343
554 Tournassat, C., Steefel, C.I., 2019. Modeling diffusion processes in the presence of a diffuse
555 layer at charged mineral surfaces: a benchmark exercise. Comput. Geosci.
556 https://doi.org/10.1007/s10596-019-09845-4
557 Tyagi, M., Gimmi, T., Churakov, S.V., 2013. Multi-scale micro-structure generation strategy
558 for up-scaling transport in clays. Adv. Water Resour. 59, 181–195.
559 https://doi.org/10.1016/j.advwatres.2013.06.002
560 van Brakel, J., Heertjes, P.M., 1974. Analysis of diffusion in macroporous media in terms of a
561 porosity, a tortuosity and a constrictivity factor. Int. J. Heat Mass Transf. 17, 1093–
562 1103. https://doi.org/10.1016/0017-9310(74)90190-2
563 Van Loon, L.R., Glaus, M.A., Müller, W., 2007. Anion exclusion effects in compacted
564 bentonites: Towards a better understanding of anion diffusion. Appl. Geochem. 22,
565 2536–2552. https://doi.org/10.1016/j.apgeochem.2007.07.008
566 Van Loon, L.R., Soler, J.M., Müller, W., Bradbury, M.H., 2004. Anisotropic Diffusion in
567 Layered Argillaceous Rocks: A Case Study with Opalinus Clay. Environ. Sci.
568 Technol. 38, 5721–5728. https://doi.org/10.1021/es049937g
569 Xiao, T., Xu, H., Moodie, N., Esser, R., Jia, W., Zheng, L., Rutqvist, J., McPherson, B., 2020.
570 Chemical-Mechanical Impacts of CO2 Intrusion Into Heterogeneous Caprock. Water
571 Resour. Res. 56, e2020WR027193. https://doi.org/10.1029/2020WR027193
572

Tracers	0MPa			1.9MPa			9MPa		
	D_e (10^{-11} m s^{-1})	α (-)	R_d (mL g^{-1})	D_e (10^{-11} m s^{-1})	α (-)	R_d (mL g^{-1})	D_e (10^{-11} m s^{-1})	α (-)	R_d (mL g^{-1})
HTO	13.7 (9.8-20.0)	0.25 (0.21-0.28)	-	4.1 (3.0-5.3)	0.22 (0.18-0.22)	-	2.0 (1.1-2.85)	0.17 (0.14-0.20)	-
HDO	-	-	-	5.1 (4.1-6.5)	0.22 (0.21-0.22)	-	1.8 (1.3-2.2)	0.17 (0.15-0.20)	-
$^{22}Na^{+}$	10.5 (8.8-13.0)	1.13 (0.98-1.35)	0.38 (0.36-0.41)	1.4 (1.25-1.56)	0.28 (0.27-0.30)	0.04	0.3 (0.25-0.35)	0.17 (0.15-0.25)	0
$^{125}I^{-}$	10.5 (9.0-12.0)	0.63 (0.60-0.65)	0.19 (0.18-0.21)	3.0 (2.0-4.9)	0.29 (0.28-0.32)	0.04	0.55 (0.35-0.80)	0.17 (0.15-0.20)	0
$^{36}Cl^{-}$	11.0 (9.0-14.5)	0.59 (0.55-0.60)	0.16 (0.14-0.17)	-	-	-	-	-	-

Table 1. *Effective diffusion coefficients, D_e, rock capacity factor, α, and distribution ratio, R_d, for HTO, HTO, $^{22}Na^{+}$, $^{125}I^{-}$ and $^{36}Cl^{-}$ estimated through compacted kaolinite for 3 suction levels of resp. 0, 1.9 and 9 MPa.*

Water tracer	$\frac{D_{e,water\ tracer}}{D_{0,water\ tracer}} / \frac{D_{e,I-}}{D_{0,I-}}$	$\frac{D_{e,water\ tracer}}{D_{0,water\ tracer}} / \frac{D_{e,Na+}}{D_{0,Na+}}$
HDO	2.91	3.53
HTO	3.23	3.92

Table 2. *Ratio between values of diffusivities for water and solute tracers at 9MPa*

		9MPa suction		1.9MPa suction	
		Values from $D_{e,Na}$	Values from $D_{e,I}$	Values from $D_{e,Na}$	Values from $D_{e,I}$
Liquid phase	θ	0.168		0.215	
	$D_{e,liq}$ (10^{-11} m s^{-1})	0.508	0.616	2.37	3.36
	$R_{d,liq}$	-		-	
Gas phase	$\phi - \theta$	0.082		0.035	
	$D_{e,gas}$ (10^{-11} m s^{-1})	7.01×10^4		3.51×10^4	
	$R_{d,gas/sol\_equi}$	134446		383474	
D_e^* (10^{-11} m s^{-1})		1.672	1.780	2.95	3.94

Table 3. *Values of parameters used in the double-diffusion model at 9MPa and 1.9MPa for water tracer*

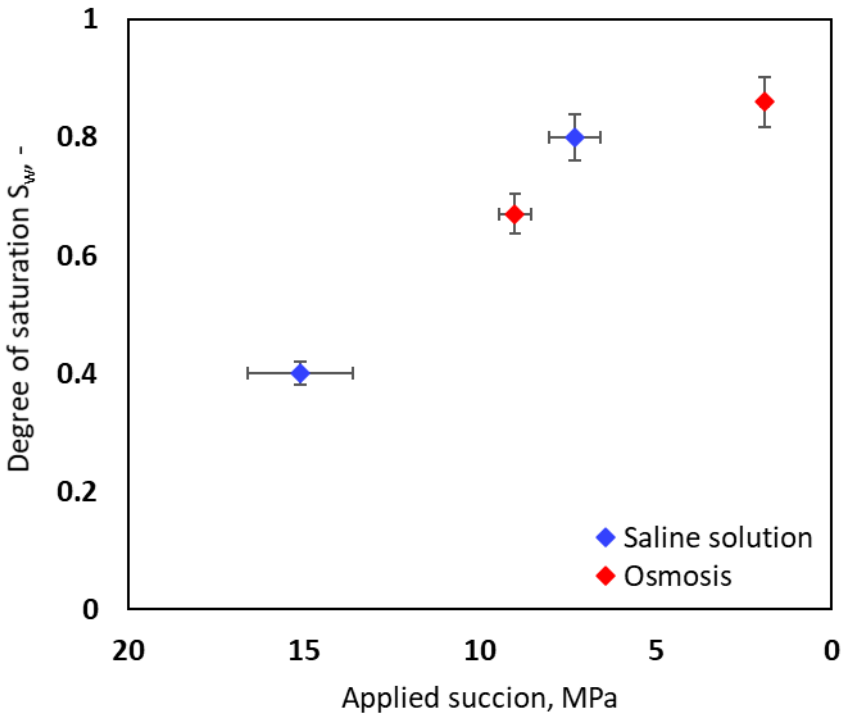

Figure 1. *Values of water saturation degree determined on kaolinite samples compacted at 1950 kg/m^3 as a function of suction applied by either osmosis method or saline solution method.*

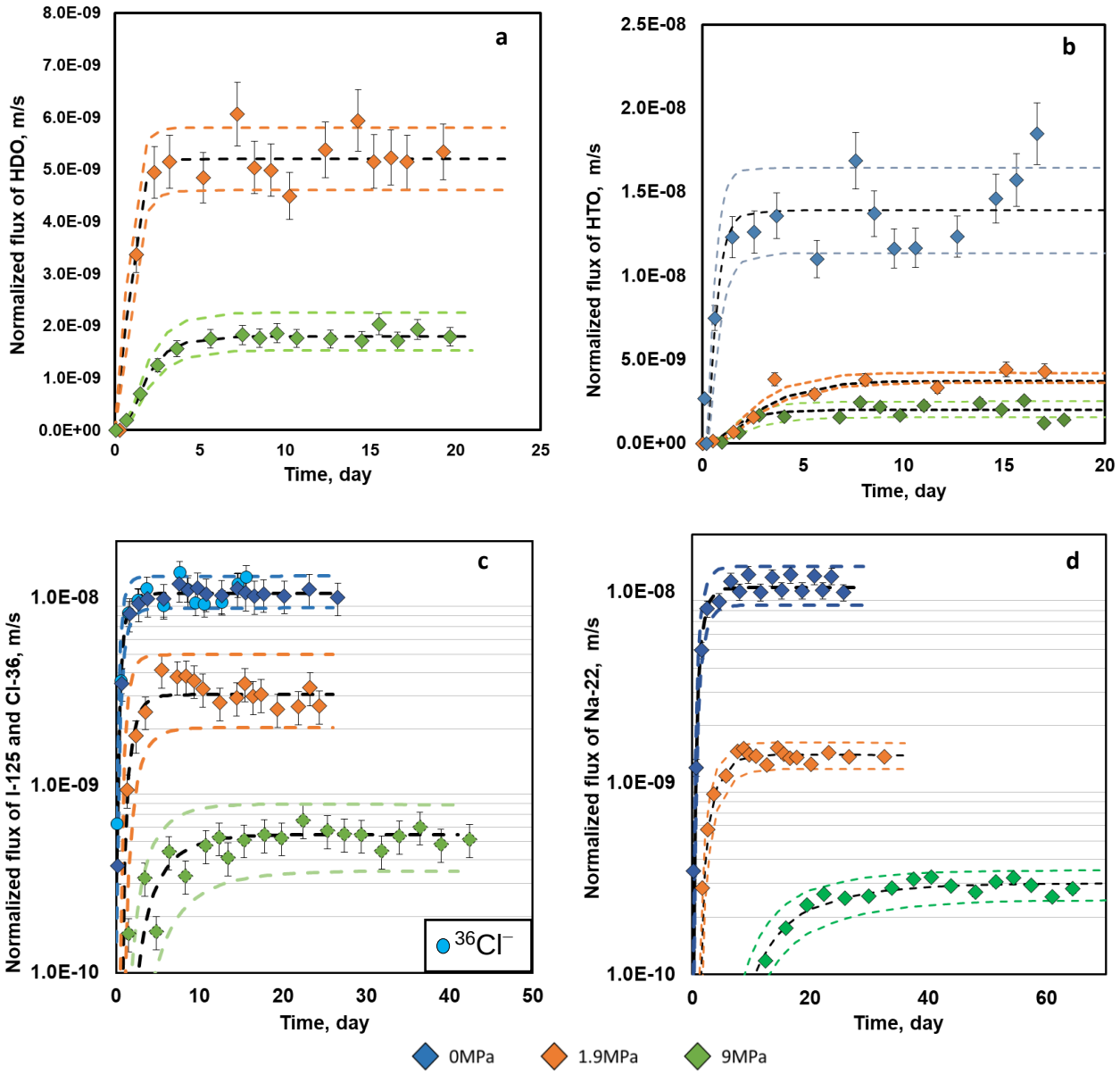

Figure 2. *Normalized diffusive fluxes for (a) HTO, (b) HDO, (c) $^{125}I^{-}$/$^{36}Cl^{-}$ and (d) $^{22}Na^{+}$ through compacted kaolinite sample, at three suction levels of resp. 0, 1.9 and 9 MPa. Note that $^{36}Cl^{-}$ was only used at 0 MPa (at full-saturation). Normalized flux is the ratio of instantaneous flux in Bq $m^{-2}s^{-1}$ (or mol $m^{-2}s^{-1}$ for HDO) over the concentration in the upstream reservoir in Bq m^{-3} or mol m^{-3}.*

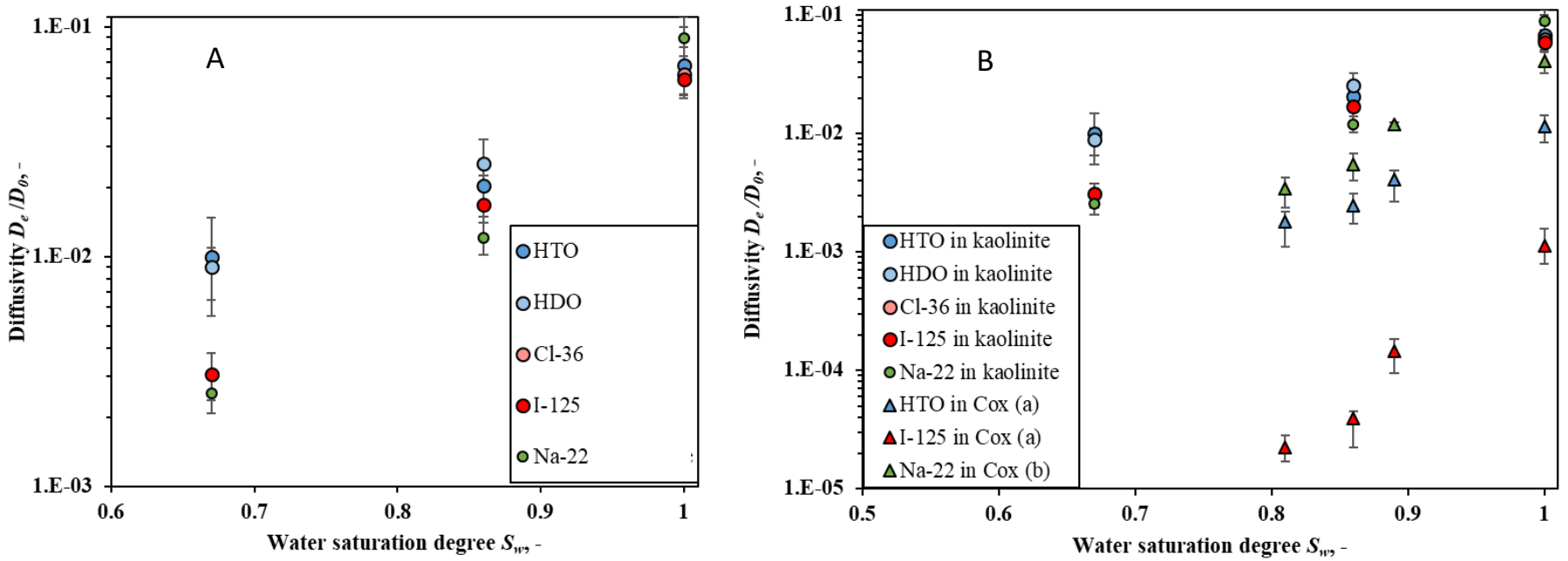

***Figure 3**. Diffusivity (D_e/D_0) as a function of water saturation degree for cation ($^{22}Na^+$), anion ($^{125}I^-$) and water tracers (HTO/HDO) for A kaolinite and comparison with data obtained in Cox in B ([a] data from Savoye et al., 2010 ; [b] data from Savoye et al., 2017).*

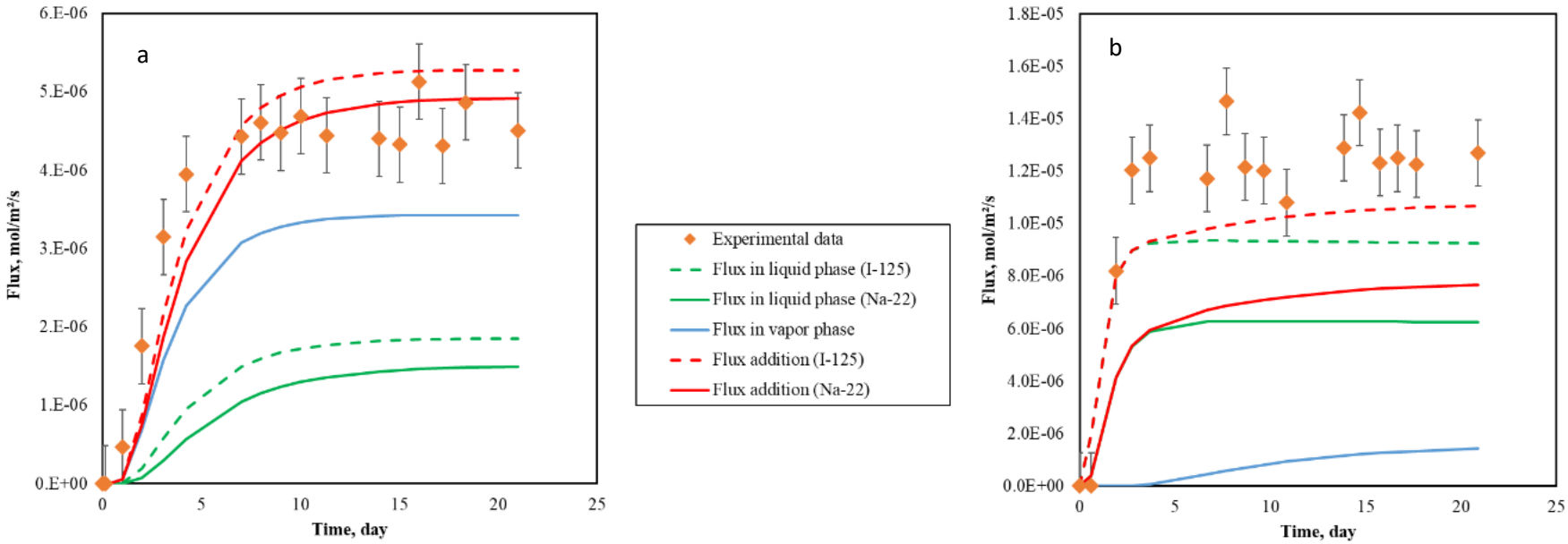

Figure 4. *Application of the double diffusion model for HDO diffusing in kaolinite under partial saturation conditions, at 9MPa (a) and 1.9MPa (b) suction levels, using either $^{22}Na^{+}$ or $^{125}I^{-}$ data for calculating HDO diffusion contribution in liquid phase and comparison with the experimental data.*